JOURNAL OF MATERIALS SCIENCE 32 (1997) 483–490

Fracture mechanics of single-fibre pull-out test

CHI WANG
Department of Chemical Engineering, Yuan-Ze Institute of Technology, Neili, Taoyuan Taiwan 320, Republic of China

Pull-out of an elastic fibre from an elastic matrix was investigated. A simple pull-out mechanics has been developed, based on the fracture energy criterion, to describe the debonding process, including friction. Experiments were carried out using polytetrafluoroethylene (PTFE) fibres embedded in a polypropylene (PP) matrix. It was found that growth of an interfacial crack was stable after the initiation of a debond at the loaded fibre end. At first, the debonding force increased linearly with the crack length due to friction in the debonded region. However, the crack accelerated after reaching a critical length, dependent on the embedded fibre length. At this point, the force required to propagate the debond levelled off. Thus, further increase in the debonding force was not necessary to further complete the debonding process. The debonding force was found to be in good agreement with that predicted by the present theory. Techniques for determining the interfacial properties, including adhesive fracture energy, compressive residual stress and coefficient of friction, were considered. In addition, a simple criterion has been derived to predict which fibre end, either embedded end or loaded end, will debond first when the specimen is subjected to an axial load.

1. Introduction

Several methods, such as fragmentation test, microbond test, and fibre pull-out test, have been developed to evaluate the bonding strength of fibre-reinforced polymer composites. Amongst these, the single-fibre pull-out test is widely used due to its simple sample preparation and measurement. The bonding strength between fibre and matrix is determined by measuring the force required to pull out a fibre embedded in the matrix. It has been pointed out that the single-fibre pull-out test can be used to evaluate interfacial properties [1] such as interfacial shear strength and frictional stress. Most of the investigators have used the interfacial shear strength as a criterion for fracture, i.e. a crack will propagate when the interfacial shear stress at the crack tip is greater than the shear strength of the interface. Thus, a number of theories have been put forward to predict the stress distribution in composites [1–5].

On the other hand, the debonding process can be treated using fracture energy as a failure criterion as well. Based on Griffith's fracture criterion [6, 7], the debonding will take place when the net available energy, i.e. the work done by the applied load minus the energy stored in the system, is larger than the work of the interfacial detachment. The work of detachment (adhesive fracture energy) is denoted by G_a, the amount of energy to separate unit area of the interface. Thus, the adhesive fracture energy is used to characterize the bonding strength.

Here, we try to elucidate the mechanics of the debonding process for an elastic fibre embedded in an elastic matrix in terms of the energetics of failure. The adhesive fracture energy and the interfacial properties of PTFE fibre/PP matrix are deduced from the single-fibre pull-out test.

2. Theoretical considerations

2.1. Initiation of a debond

When load is applied to a single-fibre composite, the shear stress developed at the interface is not constant [1–4]. It is generally accepted that interfacial debonding takes place when the interfacial shear stress exceeds the ultimate shear strength of the interface. Owing to stress concentration, there are two possible locations for a debond to initiate, i.e. either at the loaded fibre end or at the embedded fibre end, in a non-cracked specimen. Based on stress analyses, Leung and Li [2] derived a simple criterion to predict which fibre end will debond first, by comparing the interfacial shear stresses at both ends. Results showed loaded-end debonding will take place when

$$\left(\frac{R^2}{r^2} - 1\right) > \frac{E_f}{E_m} \tag{1}$$

where r is the fibre radius, R is the matrix radius, and E_f and E_m are Young's moduli of fibre and matrix, respectively. On the other hand, embedded-end debonding occurs if the ratio of E_f/E_m is greater than the value of $(R/r)^2 - 1$. The effect of Poisson's ratios of fibre and matrix was investigated by Hsueh and Becher [3], Similar results to Equation 1 were obtained. Recently, a more rigorous analysis was carried out by Fu *et al.* [4, 5] using numerical methods to

0022–2461 © *1997 Chapman & Hall*

investigate the fibre debonding and pull-out from an elastic matrix. Results showed that interfacial shear stress at the loaded end is large and a surface debond occurs when a_0 is less than 0.5*. Specifically, debonding can start at the loaded end, the embedded end or both ends, depending on the value of a_0. The parameter a_0 is a complex function of the fibre and matrix elastic properties and the fibre volume fraction.

2.2. Propagation of a debond from the embedded end

The mechanics of debonding from the embedded fibre end has been extensively investigated by Gent and co-workers [7–9]. They consider the debonding process of samples consisting of a single rigid fibre embedded in a soft block of a linearly-elastic matrix. Based on an energy criterion, the total force F_t required to propagate a debond is given by

$$F_t = 2\pi(R^2r - r^3)^{1/2}(E_m G_a)^{1/2} + 2\pi rc\tau_f \quad (2)$$

where c is the length of debond and τ_f is the frictional stress in the debonded region. The first term is denoted by F_0 and is attributed to the detachment of the fibre/matrix interface only and the second term is the contribution of the friction at the interface, assuming a constant frictional stress. Equation 2 has been verified both by experiments and by numerical simulations [8, 9].

2.3. Propagation of a debond from the loaded end

The mechanics of debonding from the loaded fibre end has been similarly investigated [10–12]. According to Equation 1, this mode of interfacial failure takes place when a relatively soft, linearly elastic fibre is embedded in an inextensible (infinite) matrix. Fig. 1b illustrates the pull-out model.

On the assumption that the energy changes both in the matrix and in the embedded fibre are negligible compared to that in the free fibre, three contributions to the energy change are involved as an increment of debonded length, Δc. First, the work done by the applied load is given by $Fe\Delta c$, where e is the tensile strain in the free fibre and is equal to $F/\pi r^2 E_f$. Second, the total strain energy stored in the fibre is increased due to the increase of the strained fibre volume, $\pi r^2 \Delta c$. Thus, the amount of increase in the strain energy is $F^2\Delta c/2\pi r^2 E_f$. Third, the energy expended in the debonding process is expressed as $2\pi r G_a \Delta c$. Using Griffith's fracture criterion, debonding takes place when the net available energy, i.e. the work done by the applied load minus the energy stored in the fibre, is larger than the work for interfacial detachment, i.e.

$$Fe\Delta c - F^2\Delta c/2\pi r^2 E_f \geqslant 2\pi r G_a \Delta c \quad (3)$$

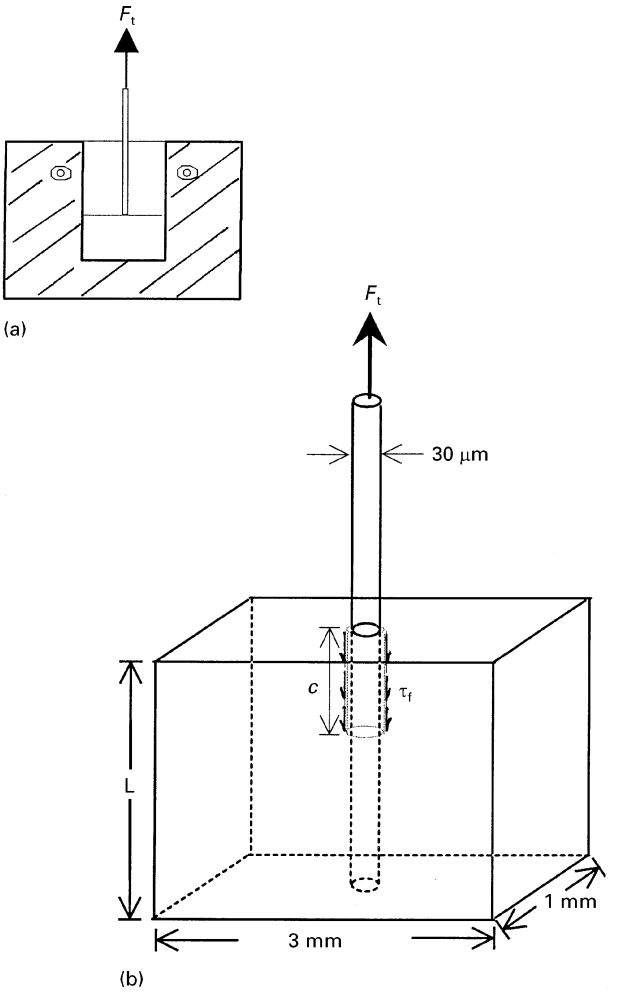

Figure 1 (a) Sketch of the clamp for pull-out test, and (b) pull-out model for specimens with embedded fibre length, L, and length of debond, c.

Thus, the pull-out force is derived to be

$$F_0^2 = 4\pi^2 r^3 E_f G_a \quad (4)$$

The pull-out force for a long debond without friction, F_0, is constant and is independent of the embedded fibre length. Equation 4 has been developed by Cherepanov [11] from stress analyses and has been verified by Morrison *et al.* [13] using finite element analyses.

When the frictional stress in the debonded region is taken into account and is assumed to be constant (which is valid only for a small debonded length; the details are discussed in Section 4.5), Equation 4 is modified, similarly to Equation 2, to be

$$F_t = 2\pi r^{3/2}(E_f G_a)^{1/2} + 2\pi rc\tau_f \quad (5)$$

According to Equations 2 and 5, a plot of measured total force versus crack length gives a straight line. By extrapolating the debonded length to zero, the debonding force in the absence of friction, F_0, is obtained and used to calculate the adhesive fracture

* a_o taken from [4], $a_0 = 1/[(R^2/r^2 - 1)m^2 + 1]$, where $m^2 = \{(1 - \upsilon_f)/E_f^2 + 1/E_f E_m [(R^2/r^2 + 1)/(R^2/r^2 - 1) + \upsilon_m] - 2\upsilon_f^2/E_f^2 - (\upsilon_f\upsilon_m)/E_f E_m)$ $[(R^2/r^2 + 1)/(R^2/r^2 - 1) - 1]\}/\{(1 - \upsilon_f)/(E_m E_f) + (1/E_m^2)[(R^2/r^2 + 1)/(R^2/r^2 - 1) + \upsilon_m] - 2\upsilon_f\upsilon_m/(E_f E_m) - (\upsilon_m^2/E_m^2)\ [(R^2/r^2 + 1)/(R^2/r^2 - 1) - 1]\}$.

energy [8]. The slope is then used to determine the frictional stress between fibre and matrix.

3. Experimental details

3.1. Materials and sample preparation

A commercial grade of polypropylene powder (Profax, PC366) without additives, supplied by Taiwan Polypropylene Co., was used as the matrix. The viscosity average molecular weight is 2.8×10^5. The melting temperature determined by DSC, with a heating rate of 10 °C min^{-1}, is 164.1 °C. The PTFE fibres were provided by Du Pont Co. The diameter is 30 μm. To make a single-fibre composite, the technique developed by Li and Grubb [14] was performed to eliminate the meniscus at the fibre ends using a silicone rubber mould to incorporate PP powder and PTFE fibre. The assembly was then heated to 200 °C for 10 min on a hot stage (Mettler, FP-82) before being quenched to 25 °C in water. The morphology of the specimens prepared in this manner was observed using a polarized optical microscope (Nikon MICROPHOT-FXA). The spherulitic radius of PP was 7 μm and the crystallinity was 41%. Detailed studies on the morphology were provided elsewhere [15]. Young's modulus and yield stress for the PP matrix were determined from the tensile stress–strain relation to be 0.72 ± 0.07 GPa and 15.3 ± 1.0 MPa, respectively. However, the PTFE fibre possessed a slightly higher Young's modulus, 0.90 ± 0.08 GPa, and a yield stress of 118 ± 19 MPa. The linear stress–strain relation was found to hold up to about 10% strain for PTFE fibre.

3.2. Measurements

The pull-out test was carried out at room temperature using an Instron tensile testing machine. A small frame, as shown in Fig. 1a, was used to fasten the specimens. The accuracy of the measured load is ± 0.3 mN. A relatively slow rate of stretching, of 1.7 μm s^{-1}, was employed. The crack growth was monitored using a microscope, video camera and recorder when the applied load was increased continuously. Owing to the rather small radius of PP spherulites which scatter the light less, the specimens were transparent. The tip of the interfacial crack was barely able to be traced under appropriate reflection of light and the debonded length was determined using a stage micrometer. Thus, the relation between load and the corresponding debonded length was recorded simultaneously. Specimens with different embedded fibre length were tested, but the width and thickness were kept constant at 3 mm and 1 mm, respectively, as shown in Fig. 1b. Each experimental result was an average of five pull-out tests.

4. Results and discussion

4.1. Observation of debonding process

It has been observed that a crack initiated at the loaded fibre end and propagated along the PTFE fibre/PP matrix interface. This is consistent with the prediction of Equation 1, taking $r = 15$ μm and equivalent radius of matrix $R = 980$ μm. Fig. 2a shows a typical force–displacement relation in the pull-out test. Similar plots for the pull-out force against the displacement have been predicted recently by numerical simulations [16]. Since the compliance of the free fibre is much greater than that of the composite, the initial linear part is due to the deformation of the free fibre. Initial debonding takes place at point A, the force being denoted by F_i, where the stiffness starts to decrease. As the debonding proceeds, the stiffness gradually decreases until at point B complete debonding occurs. The corresponding force is denoted by F_{max}, the maximum debonding force. Simultaneously, the force suddenly drops to a low value of F_f, point C. Thereafter, the fibre is sliding along the hole surrounded by matrix until at point D where the whole embedded length is pulled out from the matrix. Specimens with long embedded fibres show large force variation when the fibre slides along its entire length, Fig. 2b. This is due to the complex interaction between the elastic recovery of the strained fibre and the frictional resistance of the matrix [14]. Nevertheless, the sliding velocity of the fibre is constant (discussed next).

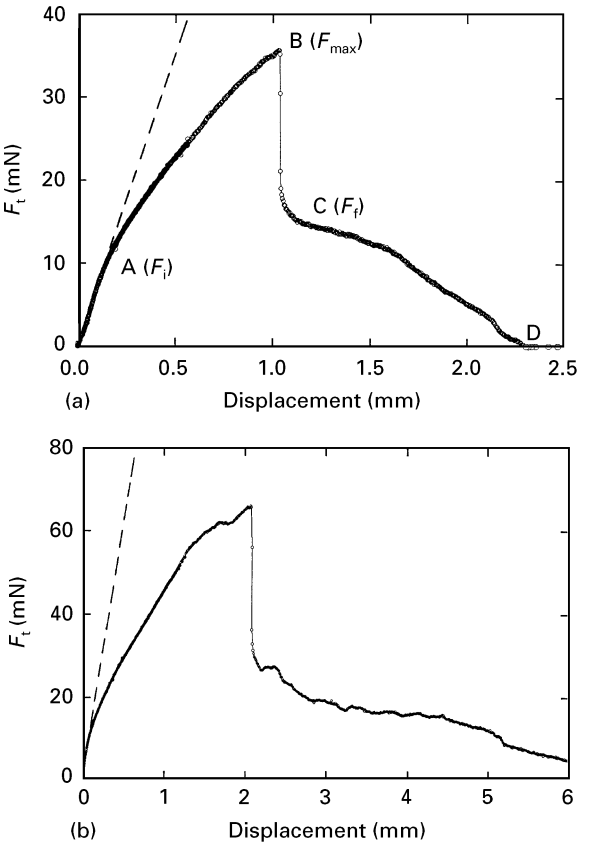

Figure 2 A typical plot of pull-out force versus displacement. (a) $L = 1.5$ mm, and (b) $L = 5$ mm.

The debonding process was monitored using a microscope under appropriate light reflection. Fig. 3 shows the photomicrographs of debonding at different stages. The debonded region appears in contrast as a bright line around the fibre surface. It was found that the fibre slips within the hole immediately after complete debonding, Fig. 3e. The amount of distance to slip depends on the value of F_{max}, i.e. the embedded

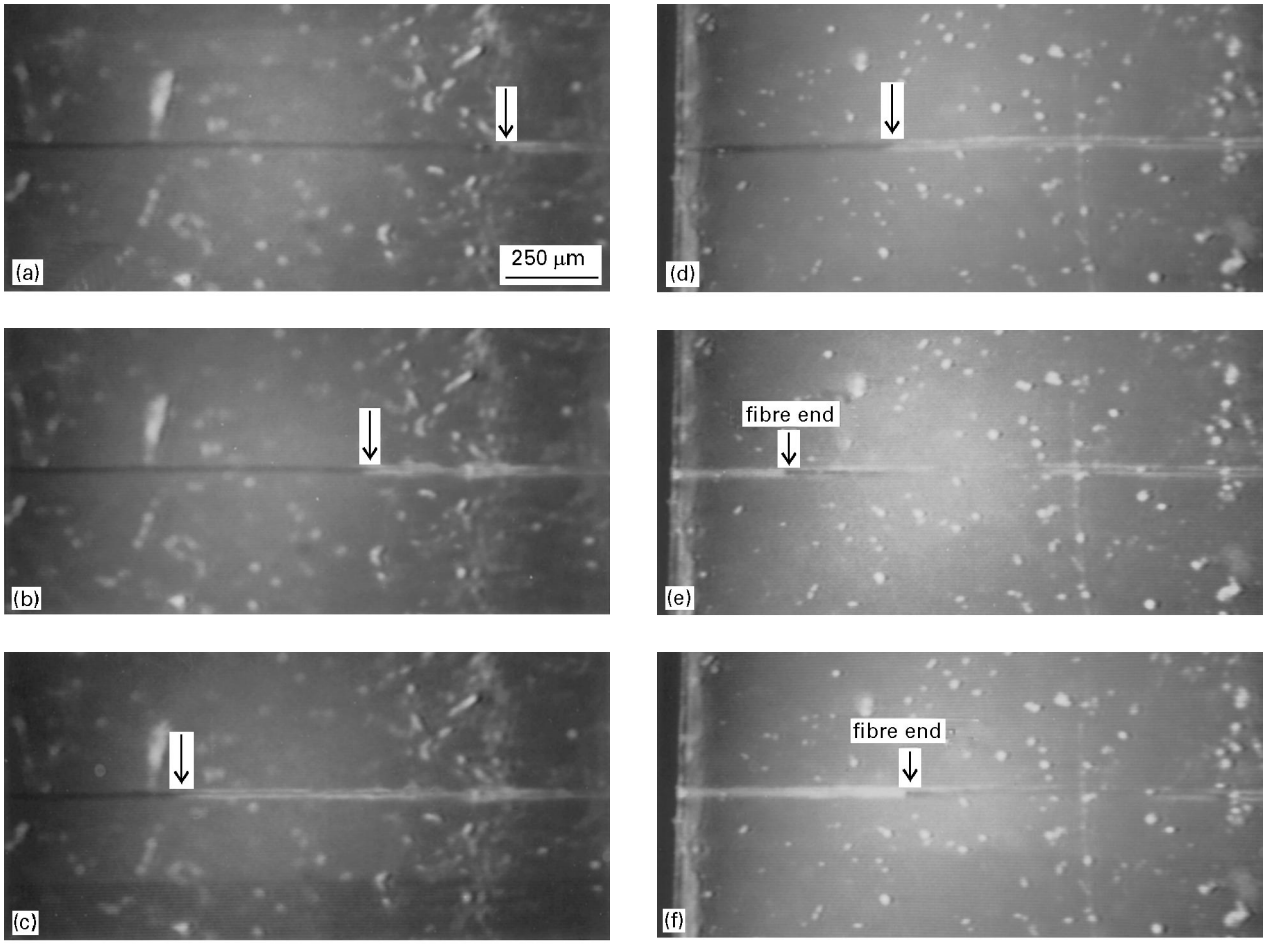

Figure 3 Photographs of debonding at different stages for specimens with $L = 4.0$ mm, (a) $c = 0.33$ mm (b) $c = 0.78$ mm (c) $c = 1.35$ mm (d) $c = 3.33$ mm (e) right after complete debonding and (f) sliding of fibre. (The load is applied to the right and the arrows point to the tip of the debond).

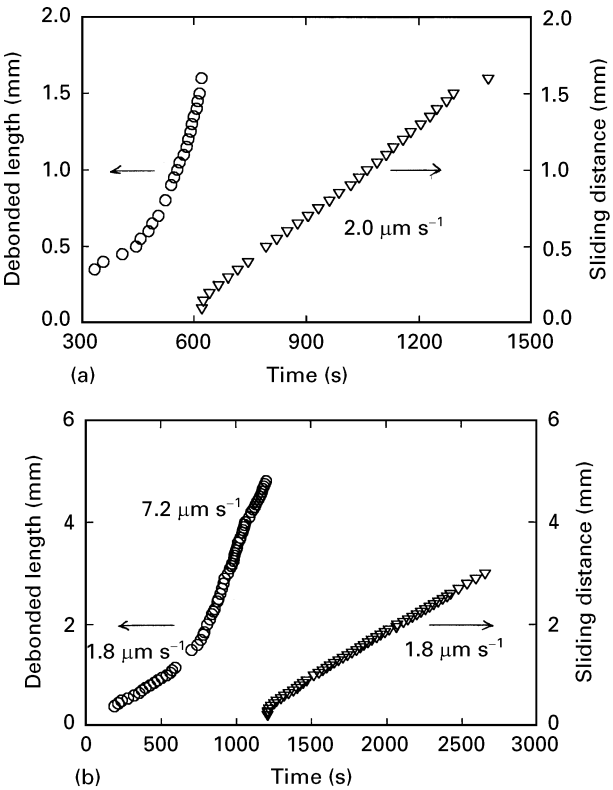

Figure 4 Measured debonded length before complete debonding and sliding distance of fibre after complete debonding as a function of time. (a) $L = 1.5$ mm, and (b) $L = 5$ mm.

fibre length. The measured debonded length was plotted against time to determine the rate of crack propagation, as shown in Fig. 4a. The initial rate of crack growth was controlled by the pulling rate of the fibre, *ca.* 1.8 μm s^{-1}. When the crack reached a critical value, a distinct change in the rate of crack growth was observed. A similar trend was found in specimens with different embedded fibre lengths, Fig. 4b. The sliding distance of the fibre, after complete debonding, was measured as well, and is also shown in Fig. 4. The sliding velocity was rather close to the pulling rate of the fibre and independent of the embedded fibre length. Thus, PTFE fibre did not exhibit stick–slip behaviour when sliding through the PP matrix. This is attributed to the fact that the static frictional coefficient of PTFE fibre is only slightly higher than the dynamic value [17].

4.2. Effect of embedded fibre length on F_i, F_{max} and F_f

Plots of measured values, F_i, F_{max} and F_f, against the embedded fibre length are shown in Fig. 5. It is noted that the debonding stress should be smaller than the yield stress of the fibre to ensure that the interfacial debonding and subsequent fibre pull-out take place. The force to yield the PTFE fibre is about 83 ± 13 mN, represented by the broken line. After the

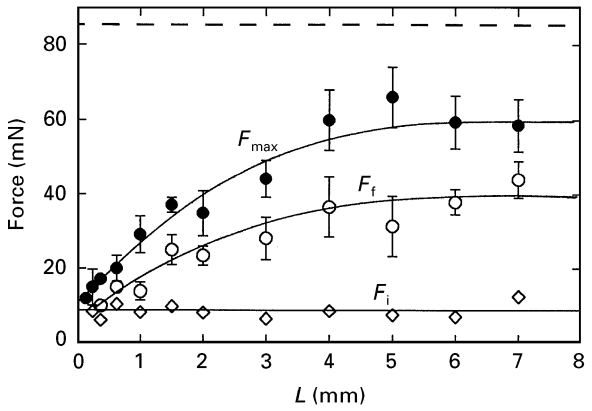

Figure 5 Variation of force to initiate a debond, F_i (◇), maximum debonding force, F_{max} (●) and the force right after complete debonding, F_f (○), with the embedded fibre length. (The broken line represents the yield force of the PTFE fibre.)

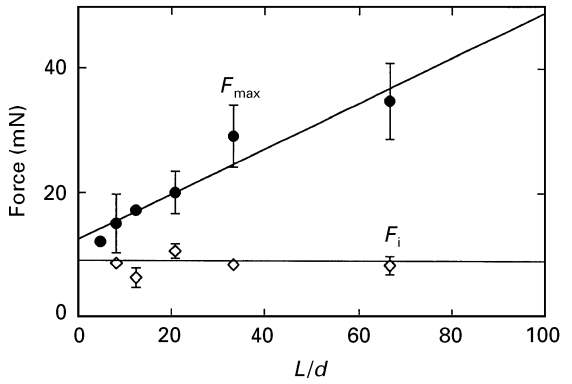

Figure 6 Plot of force versus fibre aspect ratio, L/d.

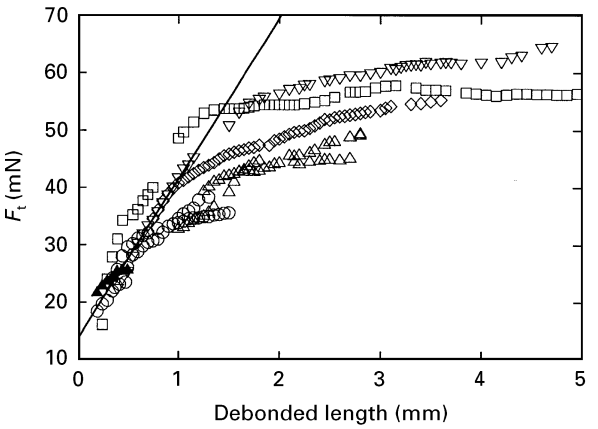

Figure 7 Total debonding force as a function of debonded length for specimens with different embedded fibre length. Key: ▲ $L = 0.6$ mm; ○ $L = 1.5$ mm; △ $L = 3.0$ mm; ◇ $L = 4.0$ mm; ▽ $L = 5.0$ mm; □ $L = 7.0$ mm.

pull-out test, the diameter and the mechanical properties of the fibre were measured. Similar results were obtained to those for PTFE fibres before test. Thus, fibre fracture was not found in the test.

It can be seen that the force required to initiate a debond, F_i, independent of the embedded fibre length, Fig. 5. The maximum debonding force, F_{max}, was found to increase with embedded fibre length. This was expected because the total debonded length is larger for specimens with longer embedded fibre length. Thus the increase in F_{max} is attributed to the friction in the debonded region. However, a plateau value of F_{max} was reached for specimens with embedded length greater than 3.0 mm. A similar relation between F_{max} and embedded length has been found in [14, 18–23]. Moreover, F_f showed the same trend as F_{max}. Values of F_f was used to estimate qualitatively the level of friction. The magnitude of F_f was about two to four times larger than F_i. Thus, the contribution of friction is significant and cannot be neglected in a pull-out test.

To calculate the adhesive fracture energy, a method to exclude the frictional effect has been suggested [13] by substituting the drop in force, $F_{max} - F_f$, into Equation 4. But, it should be noted that the fibre end extends into the hole left by the fibre for a small distance, as shown in Fig. 3e. It has observed that the slip distance was about 70 to 400 μm, depending on the maximum debonding force or the embedded length. Therefore, the real frictional force should be larger than the observed value of F_f. A method to determine the adhesion strength without a frictional effect is suggested as follows. A linear relation between F_{max} and fibre aspect ratio was found, Fig. 6, for L/d ranging from 10 to 80, where d is the fibre diameter. The slope is apparently correlated with the frictional stress, according to Equation 5 when the debonded length, c, is replaced with embedded length, L. The slope was determined to be 0.367 mN. By extrapolating the value of F_{max} to zero embedded length, the force to separate the interface in the absence of friction was obtained. The extrapolated value, F_0, is 12.4 mN which is slightly larger than the value of F_i, 9.0 mN. It is attributed to the difference in stress concentration caused by different local stress fields. To determine the effect of random data error, the average force, 10.7 mN, was applied to calculate the adhesive fracture energy using Equation 4. The values of τ_f and G_a determined in this manner are 0.13 MPa and 0.96 ± 0.32 J m^{-2}, respectively.

4.3. Determination of G_a and τ_f from Equation 5

Fig. 7 shows the variation of debonding force with the corresponding debonded length for specimens with different embedded fibre length. After a debond is initiated, the debonding force increased linearly with crack length. It is attributed to the contribution of friction in the debonded region, as predicted by Equation 5. However, the debonding force levelled off after the crack length reached a value of about 1.0 mm. At this point, the rate of crack growth was increased and led to complete debonding. Although different embedded fibre lengths were used, the intercept at zero crack length was constant, 13.6 mN. The force at zero debonded length also represents the load required to detach the interface without a frictional effect. This value was rather close to both F_0 and F_i, determined from Fig. 6. The adhesive fracture energy was determined to be 1.5 J m^{-2} from Equation 5. Moreover, the linear dependence of the force on the

crack length was constant as well, 27.9 N m^{-1}, for a debonded length smaller than 0.8 mm. The frictional stress τ_f was calculated to be 0.30 MPa, according to Equation 5. It is about twice as large as the value determined previously from the slope of the linear relation of F_{max} versus embedded length, Fig. 6. This discrepancy is due to the fact that the rate of crack growth is not constant throughout the whole debonding process, as shown in Fig. 4. Thus, the frictional stress determined from the linear dependence of F_{max} versus embedded length will be underestimated. However, the analysis from the F_{max}–L relation provides a feasible approach to estimate reasonable values of τ_f and G_a for specimens whose matrix is not transparent which makes the observation and measurement of crack growth infeasible.

4.4. Determination of residual stress and coefficient of friction

The interfacial frictional stress in the debonded region is equal to $\mu\sigma_N$, where μ is the frictional coefficient and σ_N is the normal stress acting on the fibre surface. The normal stress is given by [18]

$$\sigma_N = \sigma_r - K\sigma_f \quad (6)$$

where $K = E_m\upsilon_f/E_f(1 + \upsilon_m)$, σ_r is the residual compressive stress, σ_f is the axial stress of the fibre, and υ_f and υ_m are the Poisson's ratios of fibre and matrix, respectively. The residual compressive stress arises from the different levels of thermal shrinkage between fibre and matrix, owing to the mismatch in the thermal expansion coefficient, after the specimen is quenched from 200 to 25 °C. When a relatively large stress σ_f is applied to the fibre, the frictional stress is not constant due to the reduction of σ_N, according to Equation 6. Thus, Equation 5 is no longer valid at a large applied force which makes the Poissonian contraction of the fibre significant. Moreover, the contact between matrix and fibre disappears when the applied stress reaches a critical value at which the value of σ_N is zero. Simultaneously, the growth of the debond will accelerate without further increase in the applied stress. This was revealed by the levelling off of the debonding force for specimens with long embedded fibre length (Fig. 5) or long debonded length (Fig. 7). The residual compressive stress is determined using the plateau value of F_{max} and expressed as follows

$$\sigma_r = \frac{KF_{max}}{\pi r^2} \quad (7)$$

by taking $\sigma_N = 0$ in Equation 6. When the elastic properties are employed ($E_f = 0.9$ GPa, $E_m = 0.72$ GPa, $\upsilon_m = 0.33$, and $\upsilon_f = 0.3$), the calculated value of σ_r is 15.3 MPa.

However, effect of fibre contraction can be neglected for specimens with a small debonded length or a short embedded fibre length. In this case, the frictional stress is assumed to be constant, as discussed previously, and equal to $\mu\sigma_r$. Thus, the coefficient of friction is estimated by dividing the frictional stress at small debond, τ_f, with the residual stress. The coefficient of friction is determined to be 0.02 which is in good agreement with the reported value [17], 0.03, considering the inert nature of PTFE fibre.

4.5. Effect of Poissonian contraction of fibre

The force equilibrium between the applied stress, $\sigma_f(= F_t/\pi r^2)$, and the frictional stress, $\mu\sigma_N$, acting on a debonded length, dc, is given by

$$\pi r^2(\sigma_f + d\sigma_f) = \pi r^2\sigma_f + 2\pi r\mu(\sigma_r - K\sigma_f)dc \quad (8)$$

when Poissonian contraction of fibre is taken into consideration. Integration of Equation 8 gives

$$\frac{\sigma_r - K\sigma_f}{\sigma_r - K\sigma_o} = \exp(-2\mu Kc/r) \quad (9)$$

using a boundary condition: the force to initiate a debond is given by Equation 4, i.e. $\sigma_f = \sigma_o = 2(E_fG_a/r)^{0.5}$ at $c = 0$. Equation 9 is valid for the whole debonding process while Equation 5 is only applied to initial debonding where the debonded length is small. After substituting the values ($\sigma_r = 15.3$ MPa, $\sigma_o = 19.2$ MPa, and $K = 0.18$ determined previously) in Equation 9, the effect of frictional coefficient on the debonding force is as shown in Fig. 8. The total debonding force, F_t, increases with the coefficient of friction. Moreover, the length of debond to reach the plateau of F_t decreases with increasing coefficient of friction. It is consistent with the numerical results predicted by Fu *et al.* [5]. Fig. 8 also shows the results of experimental measurements of specimens with $L = 7$ mm. It is obvious that better agreement is achieved when $\mu = 0.05$ is used. This is close to the value obtained by the method stated in Section 4.4.

According to Equation 9, two important interfacial parameters must be considered to predict the relation between pull-out force and displacement, Fig. 2. One is the residual stress, σ_r, and the other is the bonding stress at the interface, represented by σ_o. When the value of σ_r/K is larger than σ_o value, the total resistance to pull-out, F_t, increases with the debonded length. This is the case for the present work. Observation of the crack growth is possible under appropriate

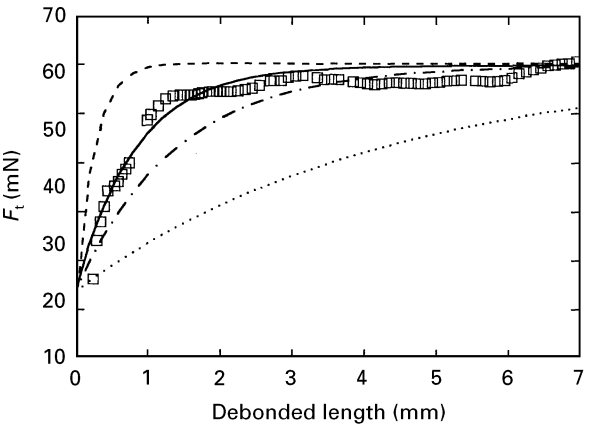

Figure 8 Effect of frictional coefficient on the total debonding force for specimens with $L = 7$ mm. Key: – – – $\mu = 0.10$; —— $\mu = 0.05$; –·– $\mu = 0.03$; · · · · $\mu = 0.01$.

control, as shown in Fig. 3. Conversely, the debonding force is decreased with debonded length when σ_r/K value is smaller than σ_o value. A catastrophic growth of debond takes place once a crack initiates at the fibre end. Only the maximum debonding force can be recorded on the force–displacement curve [24] without changing in stiffness at the AB region, as shown in Fig. 2. Therefore, the observation of crack growth is not possible.

4.6. Which end of the fibre will debond first?

The forces to propagate a debond in the absence of friction are given by Equations 2 and 5, taking $c = 0$, for a debond starting from the embedded end and from the loaded end, respectively. They are also used to estimate the forces needed to initiate a debond if the intensity of stress singularity both at the crack tip and near the fibre end is not taken into consideration. Therefore, by comparing the fracture forces, a transition from embedded-end debonding to loaded-end debonding is expected to occur,

$$2\pi(R^2r - r^3)^{1/2}(E_mG_a)^{1/2} > 2\pi r^{3/2}(E_fG_a)^{1/2} \quad (10)$$

The result is exactly the same as Equation 1 which has been derived by Leung and Li [2] using complicated stress analyses to calculate the interfacial shear stress distribution. However, a shear strength debonding criterion was applied in their modelling of the debonding process. Our analyses were based on a fracture energy criterion, using G_a to characterize the strength of the interface. Thus, both approaches come to the same conclusion in predicting which fibre end will debond first. The present work shows that the adhesive energy-based theory provides a concise analysis.

Fig. 9 shows the comparison of the debonding transition predicted both by Equation 1 (solid line) and by numerical analyses [4] (data symbols). In the numerical analyses, a complex parameter a_0 was used, as defined earlier, to predict the debonding mode. In other words, embedded-end debonding occurs when a_0 is larger than 0.5. On the other hand, loaded-end debonding takes place when a_0 is smaller than 0.5. It can be seen that Equation 1 is identical to that derived by the a_0 parameter if $\upsilon_f = \upsilon_m = 0.33$. Furthermore, the effect of Poisson's ratios, both υ_f and υ_m, on the transition is insignificant. This is consistent with the previous work by Hsueh and Becher [3]. In general, embedded-end debonding occurs when the Young's modulus of the fibre is much higher than that of the matrix. The steel wire/rubber system is such a case which has been investigated in detail by Gent and co-workers [7–9]. In most polymer composite systems, however, loaded-end debonding is usually observed [14, 23] due to the relatively small value of the fibre radius and comparable values of E_f to E_m.

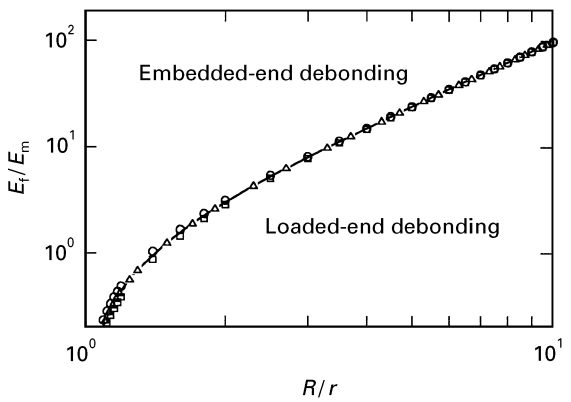

Figure 9 Relation of E_f/E_m with R/r for a transition from embedded-end debonding to loaded-end debonding. (The solid line is predicted by Equation 1, and symbols are obtained using the parameter a_0 derived by Fu *et al.* [4]. △: $\upsilon_f = 0.33$, $\upsilon_m = 0.33$; ○: $\upsilon_f = 0.33$, $\upsilon_m = 0.5$; □: $\upsilon_f = 0.5$, $\upsilon_m = 0.33$.)

5. Conclusions

The mechanics of the debonding process, starting either from the embedded end or from the loaded end, in the pull-out test can be well defined using a fracture energy criterion. The pull-out force in the absence of friction is found to be independent of the embedded fibre length, as predicted by Equations 2 and 4 for each debonding failure. But, the apparent maximum debonding force increases with the embedded fibre length. It is attributed to the friction between fibre and matrix in the debonded region. The contribution of friction to the total debonding force can be as large as that of detachment of the interface. It has been found that after a debond reaches a critical size, further increase in the debonding force is not necessary to advance the failure. Moreover, the value of F_{max} reaches a plateau value for specimens with a rather long embedded fibre length. It is attributed to the Poissonian contraction of the fibre in the debonded region which reduces the normal stress acting on the fibre and the effect of friction. In general, adhesive fracture energy, coefficient of friction and the residual compressive stress can be deduced from a single-fibre pull-out test.

Acknowledgements

The financial support of this work by National Science Council (NSC85-2216-E-155-003) is greatly appreciated. The author is also indebted to Professor A. N. Gent for helpful discussions.

References

1. C. Y. YUE and W. L. CHEUNG, *J. Mater. Sci.* **27** (1992) 3173.
2. C. K. Y. LEUNG and V. C. LI, *ibid.* **26** (1991) 5996.
3. C. H. HSUEH and P. F. BECHER, *J. Mater. Sci. Lett.* **12** (1993) 1933.
4. S. Y. FU, B. L. ZHOU, X. CHEN, C. F. XU, G. H. HE and C. W. LUNG, *Composites* **24** (1993) 5.
5. S. Y. FU, B. L. ZHOU, X. CHEN, G. H. HE and C. W. LUNG, *ibid.* **24** (1993) 13.
6. A. A. GRIFFITH, *Phil. Trans. R. Soc.* **221** (1920) 163.
7. A. N. GENT, G. S. FIELDING-BUSSELL, D. I. LIVINGSTON and D. W. NICHOLSON, *J. Mater. Sci.* **16** (1981) 949.
8. A. N. GENT and G. L. LIU, *ibid.* **26** (1991) 2467.
9. A. N. GENT and C. WANG, *ibid.* **28** (1993) 2494.
10. C. GURNEY and J. HUNT, *Proc. R. Soc.* **A299** (1967) 508.
11. G. P. CHEREPANOV, "Mechanics of Brittle Fracture" (McGraw-Hill Book Co., Inc., New York, 1979).

12. H. STANG and S. P. SHAH, *J. Mater. Sci.* **21** (1986) 53.
13. J. K. MORRISON, S. P. SHAH, and Y-S. JENQ, *J. Eng. Mech. ASCE* **114** (1988) 277.
14. Z-F. LI and D. T. GRUBB, *J. Mater. Sci.* **29** (1994) 189.
15. C. WANG and L. M. HWANG, *J. Polym. Sci.*: *Part B*: *Polym. Phys*., **34** (1996) p 1435.
16. A. HAMPE, G. KALINKA, S. MERETZ, and E. SCHULZ, *Composites* **26** (1995) 40.
17. B. J. BRISCOE, C. M. POOLEY, and D. TABOR, in "Advances in Polymer Friction and Wear", Vol. 5A, edited by L. H. Lee (Plenum Press, NY, 1975). Reported value of 0.003 by Du Pont Co. using thrust washer test.
18. A. TAKAKU and R. G. C. ARRIDGE, *J. Phys. D* **6** (1973) 2038.
19. R. J. GRAY, *J. Mater. Sci.* **19** (1984) 1680.
20. C. Y. YUE and L. CHEUNG, *ibid.* **27** (1992) 3181.
21. P. S. CHUA and M. R. PIGGOTT, *Compos. Sci. Technol.* **22** (1985) 107.
22. M. R. PIGGOTT and M. M. REBOREDO, *Compos. Interface* **2** (1994) 457.
23. X. H. GU, R. J. YOUNG and R. J. DAY, *J. Mater. Sci.* **30** (1995) 1409.
24. G. DESARMOT and J.-P. FAVRE, *Compos. Sci. Technol.* **42** (1991) 151.

Received 20 October 1995
and accepted 13 June 1996